Gearbox damage identification and quantification using stochastic resonance

Mechanics & Industry **18**, 805 (2017)
© AFM, EDP Sciences 2017
https://doi.org/10.1051/meca/2017041

Mechanics & Industry

Available online at:
www.mechanics-industry.org

**Experimental Vibration Analysis**

Regular Article

# Gearbox damage identification and quantification using stochastic resonance

Clement U. Mba*, Stefano Marchesiello, Alessandro Fasana, and Luigi Garibaldi

Dynamics & Identification Research Group, Department of Mechanical and Aerospace Engineering, Politecnico di Torino, Corso Duca degli Abruzzi 24, 10129 Torino, Italy

Received: 12 December 2016 / Accepted: 6 November 2017

**Abstract.** Amongst the many new tools used for vibration based mechanical fault diagnosis in rotating machineries, stochastic resonance (SR) has been shown to be able to identify as well as quantify gearbox damage via numerical simulations. To validate the numerical simulation results that were obtained in a previous work by the authors, SR is applied in the present study to data from an experimental gearbox that is representative of an industrial gearbox. Both spur and helical gears are used in the gearbox setup. While the results of the direct application of SR to experimental data do not exactly corroborate the numerical simulation results, applying SR to experimental data in pre-processed form is shown to be quite effective. In addition, it is demonstrated that traditional statistical techniques used for gearbox diagnosis can be used as a reference to check how well SR performs.

**Keywords:** Stochastic resonance / Damage identification and quantification / pre-processed signals

## 1 Introduction

In industries, maintenance is periodically performed on machineries in order to reduce the chances of catastrophic failure. Economically, this is an effective cost saving measure and there is no doubt that vibration based condition monitoring plays a key role in both preventive and predictive maintenance of rotating machineries. It is due to this fact that many methodologies for performing vibration based condition monitoring exist, some of which are quite new.

Stochastic resonance (SR) is a fairly new approach in the sense that it has only been used recently for fault detection in mechanical systems. It stands out from other techniques because it is able to use the noise in a system to its advantage [1]. This means that while other approaches rely on some form of filtering to work effectively, SR makes use of noise as part of its functionality. Researches that have been conducted so far on the application of SR to mechanical systems have shown promising results [2–6] and thus, it remains an area of vital interest.

In [3,4], SR is applied to impact signals generated by the simulation of a set of spur gears in mesh. The simulation is done using the equations of motion and taking the varying meshing stiffness of the meshing gears into account. Furthermore, the transmission path between the gear meshing points and the transducers are considered. In the work, different number of signal cycles, fault severities and noise levels are tested to see how well SR performs for the simulated data. The results in the work show that SR is quite effective for the simulated gearbox vibration data. The work in this article goes a step further by applying SR to real life vibration data from a gearbox. The gearbox data is obtained from the prognostics and health management (PHM) dataset 2009 [7] where a double stage reduction gearbox with different types of faults is run at different speeds under both high and low loads. More details about the gearbox setup is described in Section 3. Additionally, SR is applied to the most common statistical techniques used for gearbox diagnosis with the results compared.

## 2 Brief description and application of stochastic resonance

SR is a non-linear time domain signal processing technique that uses a proper amount of noise to amplify and detect a weak signal. It was first used within the framework of the earth's climate [8] but it has seen usage in other fields such as biology, physics, finance and engineering [9]. In the context of condition monitoring, SR refers to a scenario where non-linear system noise is used to enhance the signal to noise ratio (SNR) output of the system. Generally, a periodic input, inherent noise and system threshold are required for SR to occur. These features cause a resonance

* e-mail: clement.mba@polito.it

like behavior response of the non-linear system as a function of noise, thus the name stochastic resonance [10]. SR is a unique feature extraction procedure in the sense that it requires the presence of noise to produce desired results. In addition, it is governed by a simple equation which is described by the Brownian motion equation of particles:

$$\frac{\mathrm{d}x}{\mathrm{d}t} = -\frac{dU(x)}{\mathrm{d}x} + s(t) + n(t), \tag{1}$$

where $U(x)$ is the potential function, $s(t)$ is the input signal and $n(t) = \sqrt{2D}\varepsilon$ is the input noise which can either be inherent or synthetic, with $D$ being the noise intensity and $\varepsilon$ the Gaussian noise. $U(x)$ which is a reflection-symmetric quartic potential is given by

$$U(x) = -\frac{1}{2}ax^2 + \frac{1}{4}bx^4. \tag{2}$$

Combining equations (1) and (2), the following equation is obtained:

$$\frac{\mathrm{d}x}{\mathrm{d}t} = ax - bx^3 + s(t) + n(t), \tag{3}$$

$a$ and $b$ are the non-linear system parameters that are responsible for SR occurrence and they can be adjusted in such a way that the full effect of SR is obtained. Hence whether SR occurs depends on $a$ and $b$. In order to really understand how SR works, let us consider Figure 1. Figure 1 shows a double well symmetric potential at different states a, b, c and d. In the first state a, there is a ball otherwise called a brownian ball in the left side well. When a periodic input signal is applied to this potential, both wells modulate but the ball remains in the left side well. When a proper amount of noise is combined with the periodic input signal, the addition of noise provides the energy for the ball to move to the next well which is what happens in states b, c and d. In the absence of both the signal and noise, the state of the potential depends on initial conditions. If state a is the original state of a particular system, the non-linear system parameters a and b can be adjusted in such a way that the ball jumps to the height of the barrier that separates the left side well from the right side well, without getting into the right side well but instead returns to its original position in the left side well. This incident leads to a huge spike that can be quantified by a performance indicator such as kurtosis and used to detect hidden impulses in a noisy signal as shown in Figure 2.

An impulse response function (IRF) submerged in noise can be seen at the top of Figure 2. This combination of IRF and noise corresponds to $s(t) + n(t)$ in the SR equation (3). In the bottom figure of Figure 2, the SR output which is given by $x$ in the SR equation (3) can be seen. This output can be obtained by solving equation (3) numerically bearing in mind that the non-linear system parameters $a$ and $b$ have to be well tuned. When this is well executed, the impulse which was originally hidden in the top figure is made very conspicuous in the bottom figure. It can also be seen that there is a very huge amplification in the kurtosis which is used here as a performance indicator. The green horizontal line in the bottom figure corresponds to the left well of the potential and it is given by $-\sqrt{\mathrm{a/b}}$, while the red horizontal line corresponds to the right well of the potential and it is given by $\sqrt{\mathrm{a/b}}$. In addition, the threshold of the potential is given by the vertical distance from either the green horizontal line or the red horizontal line to zero. The height of the potential barrier $\Delta U$, shows the following relationship between the non-linear system parameters $a$ and $b$.

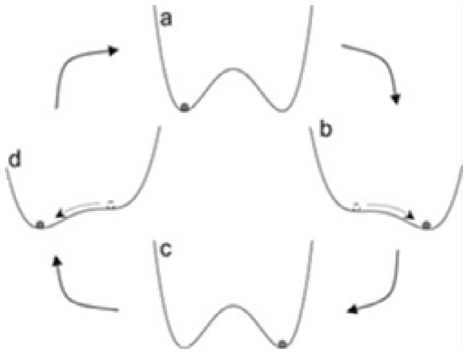


**Fig. 1.** Bistable system showing brownian particle motion in the presence of a periodic input signal and noise [2].

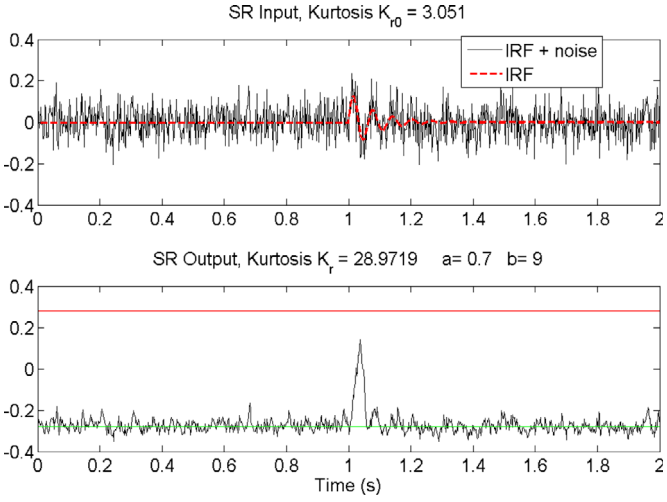


**Fig. 2.** Example of results that can be obtained when the non-linear system parameters a and b are well tuned [2]. The green horizontal line in the bottom figure corresponds to the left well of the potential while the red horizontal line corresponds to the right well of the potential.

$$\Delta U = \frac{a^2}{4b}. \tag{4}$$

In addition to properly tuning the non-linear system parameters $a$ and $b$, there are requirements that have to be met in a system for the SR equation to work. These include having a low amplitude, low frequency and low noise intensity of the input signal. However in reality, practical systems generally do not meet these requirements. As a result, the input signal is usually subjected to preprocessing techniques like re-scaling frequency, normalization, modulation, etc., before the SR equation is applied. Further-

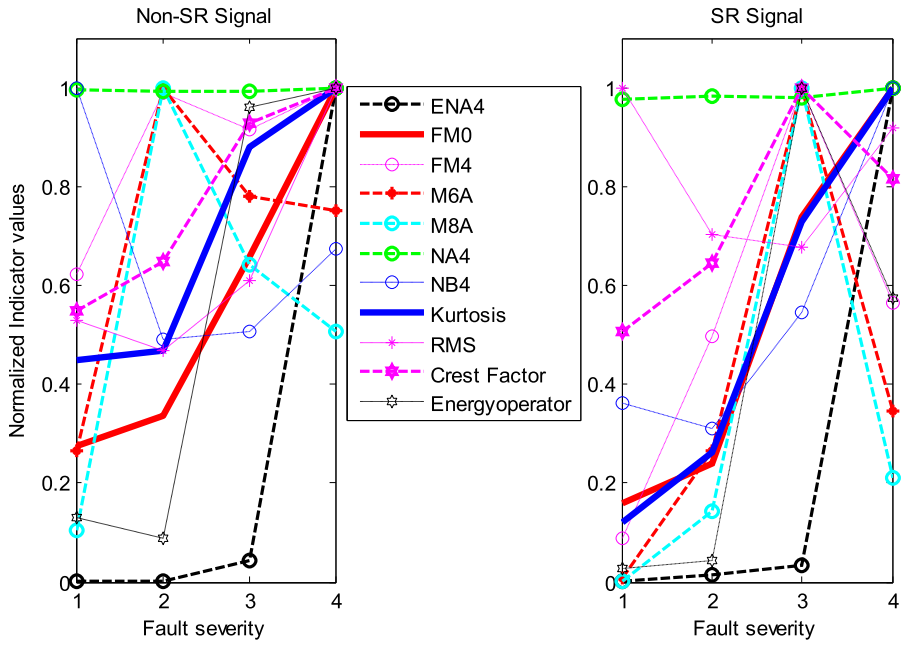


**Fig. 3.** Comparison of the changes in the most common gearbox fault diagnosis statistical features. (a) non-SR Signal (b) SR Signal.

more, there have been questions on how to properly tune the non-linear system parameters $a$ and $b$. Different methodologies such as Resonance Curve [2], Ant Colony Optimization [6], Particle Swarm Optimization (PSO) [11], Standard Differential Evolution (SADE) [12] and grey wolf optimization [13] have been put forward in literature with good results. The commonly used procedure which is really simple to apply is the kurtosis maximization algorithm which is typically applied after normalizing the input signal with a certain standard deviation. The kurtosis maximization algorithm is employed in this work.

With a view to showing the effect of SR as a possible amplifier, Figure 3 shows the changes that traditional statistical features for gearbox diagnosis undergo for both SR and non-SR signals as the fault severity progresses. Note that the vibration data used for analyses here is obtained by means of the simulation methodology described in the introduction. The statistical features [14–16] are defined as follows:

### 2.1 Root mean square

The root mean square (RMS) gives a measure of the power content in a vibration signature. It is given by

$$\mathrm{RMS} = \sqrt{\left(\frac{1}{N}\sum_{n=1}^{N} x_n^2\right)},$$

where $N$ is the number of samples and $x_n$ is the data series.

### 2.2 Kurtosis

Kurtosis is defined as the fourth normalized moment of a given distribution. It gives a measure of the "peaked ness" of the probability distribution of a real valued random variable. Kurtosis is perhaps the most commonly used statistical indicator for fault diagnosis in the time domain. Its definition is given by

$$\frac{\mathrm{Kurtosis} = N\sum_{n=1}^{N}(x_n - x)^4}{[\sum_{n=1}^{N}(x_n - x)^2].}$$

### 2.3 Crest factor

Crest factor is defined as the ratio of the maximum positive amplitude of the input signal to the RMS of the input signal. Its definition is

$$\mathrm{Crest\,Factor} = \frac{\max[\mathrm{abs}(x_n)]}{\mathrm{RMS}(x_n)}.$$

### 2.4 Energy operator

The energy operator is calculated by taking the normalized kurtosis of value $x_n^2 - (x_{n-1} * x_{n+1})$ for every point $x_n$ of the signal $x$ in a continuous loop.

### 2.5 FM0

FM0 is defined as the ratio of the peak-to-peak level of the Time Synchronous Average signal to the sum of the amplitudes of the mesh frequencies and their harmonics. The TSA signal is acquired by synchronous averaging of the raw signal with a signal that is synchronous with the desired signal, or a repetitive frequency of the desired signal (like the tachometer signal) [15,17–19]. There are four general steps involved in generating the TSA signal:

– Calculate the zero crossings corresponding to one shaft revolution from the tachometer signal that is synchronous with the shaft.

– Perform interpolation to increase the number of data points in the series generated in the first step.
– Use the results of the second step to resample the original acceleration signal. This is otherwise known as order tracking.
– Divide the order-tracked signal into segments of equal length and find the average. This average is known as the TSA and it is periodic. Subtracting the TSA from the original acceleration signal gives the random noisy part of the original acceleration signal.

TSA is quite important because it is the basis for various gear and shaft condition-monitoring algorithms like the FM0. FM0 is given as

$$\mathrm{FM0} = \frac{\mathrm{PPA}}{\sum_0^h A_n},$$

where PPA is the peak-to-peak amplitude of the TSA signal, $A_n$ is the amplitude of the $n$th harmonic and $h$ is the total number of harmonics.

### 2.6 FM4

FM4 is the kurtosis of the difference signal and it is given as

$$\frac{\mathrm{FM4} = N\sum_{n=1}^{N}(d_n - d)^4}{[\sum_{n=1}^{N}(d_n - d)^2]},$$

where $d_n$ is the data series of the difference signal and $\tilde{d}$ is the mean value of the difference signal. The difference signal is determined by removing the mesh frequencies and their harmonics, the shaft frequencies and their harmonics, and the first order sidebands from the original time synchronous averaged signal [14–16]. When only the mesh frequencies and their harmonics are removed along with the shaft frequencies and their harmonics from the original time synchronous averaged signal, the resulting signal is known as a residual signal. That is to say that the only difference between the residual signal and difference signal is the presence of first order sidebands in the residual signal.

### 2.7 NA4

NA4 is defined as the ratio of the fourth statistical moment of the residual signal to the square of its run time averaged variance. It is given as

$$NA4 = \frac{N\sum_{n=1}^{N}(r_{nM} - \tilde{r_M})^4}{\left(\frac{1}{M}\sum_{k=1}^{M}[\sum_{n=1}^{N}(r_{nk} - \tilde{r_k})^2]\right)^2},$$

where $r$ is the residual signal, $\tilde{r}$ is the mean value of the residual signal, $k$ is the index of the time signal in the run ensemble and $M$ is the current time signal number.

### 2.8 NA4*

NA4* otherwise known as ENA4 is an enhanced version of NA4. It is obtained by dividing the normalized fourth statistical moment of the residual signal by the residual signal variance for a healthy gearbox. The equation for NA4* is as follows

$$\frac{\mathrm{NA4*} = \frac{1}{N}\sum_{n=1}^{N}(r_n - r)^4}{(V)^2},$$

where $V$ is the variance of the residual signal of the healthy gearbox.

### 2.9 M6A

M6A is determined by normalizing the sixth variance of the difference signal to its variance of the third power. It is given as

$$\frac{\mathrm{M6A} = N^2\sum_{n=1}^{N}(d_n - d)^6}{[\sum_{n=1}^{N}(d_n - \tilde{d})^2]^3}.$$

### 2.10 M8A

M8A is determined by normalizing the eighth variance of the difference signal to its variance of the fourth power. It is given as

$$\frac{\mathrm{M8A} = N^3\sum_{n=1}^{N}(d_n - d)^8}{[\sum_{n=1}^{N}(d_n - \tilde{d})^2]^4}.$$

### 2.11 NB4

NB4 is similar to NA4 except that it makes use of the envelope of the signal band-pass filtered about the mesh frequency. The equation for NB4 is as follows

$$\frac{\mathrm{NB4} = N\sum_{n=1}^{N}(E_{nM} - E_M)^4}{\left(\frac{1}{M}\sum_{k=1}^{M}[\sum_{n=1}^{N}(E_{nk} - \tilde{E}_k)^2]\right)^2},$$

where $E$ is the envelope of the band-pass filtered signal. The envelope is computed in the following way

$$E = \sqrt{B^2 + H[B]^2},$$

where $B$ is the band-pass filtered signal and $H[B]$ is its Hilbert transform.

On the x axes of Figure 3, 1 corresponds to a healthy case, 2 corresponds to a small fault case, 3 corresponds to a medium fault case and 4 corresponds to a large fault case. Figure 3a shows the changes that occur when the statistical indicators are applied directly to the raw signal and Figure 3b shows the changes that occur when the statistical indicators are applied to the output of the SR system after the raw signal is passed through the SR system. As can be seen with some of the indicators, SR tends to amplify the absolute changes that occur in all or some stages of fault growth. This is particularly true for the kurtosis, crest factor, FM0, FM4, M6A, NB4, M8A, ENA4 and energy operator. In general, the kurtosis and FM0 provide the

**Table 1.** showing geometry of double stage reduction gearbox.

| | Spur gear | Angular speed | Helical gear | Angular speed |
|---|---|---|---|---|
| Input shaft: input pinion | 32 teeth | 30 Hz | 16 teeth | 30 Hz |
| Idler shaft: 1st idler gear | 96 teeth | 10 Hz | 48 teeth | 10 Hz |
| Idler shaft: 2nd idler gear | 48 teeth | 10 Hz | 24 teeth | 10 Hz |
| Output shaft: Output gear | 80 teeth | 6 Hz | 40 teeth | 6 Hz |

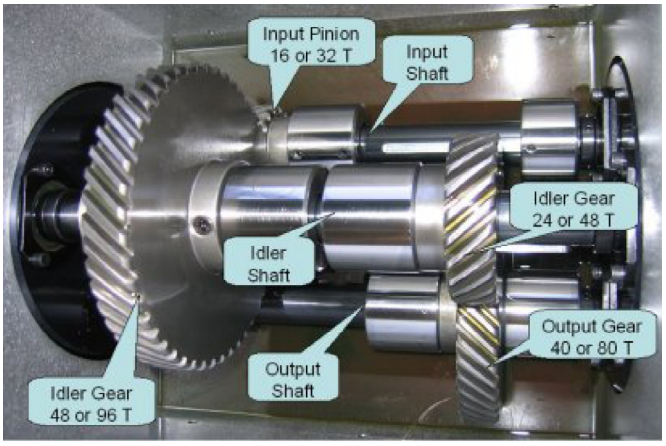


**Fig. 4.** Double stage reduction gearbox [7].

clearest indication of these changes; however, the overall amplification is greater in the kurtosis than in any of the other indicators. This either shows that kurtosis might be the most suitable indicator for SR in the time domain, or could be as a result of using the kurtosis maximization technique.

## 3 Experimental setup, results and analyses

In this section, SR is applied to experimental data obtained from the double stage reduction gearbox described in [7] and shown in Figure 4. At both high and low loads, the gearbox is run at different angular speeds of the input shaft (30 Hz, 35 Hz, 40 Hz, 45 Hz, and 50 Hz) with data collected at each speed and load. In addition, the runs are repeated twice for each load and speed. Both spur gears and helical gears are used separately in the setup of the gearbox to obtain different data as depicted in Table 1. Table 2 shows the different configurations and fault severities of the double stage reduction gearbox data analyzed in this work. For the initial test in this work, we analysed the first-run data with an input shaft speed of 30 Hz and high load. Future works will focus on repeating the same tests carried out here on the other gearbox data and subsequently, use the results obtained for the validation of the results obtained here.

As shown in Table 1, the gear ratio between the input shaft and the idler shaft is $\frac{96}{32}$ or $\frac{48}{16} = 3:1$ and the gear ratio between the idler shaft and the output shaft is $\frac{80}{48}$ or $\frac{40}{24} = 1.67:1$. Therefore, the overall reduction ratio for both gear setups are the same: $\frac{32}{96} * \frac{48}{80}$ or $\frac{16}{48} * \frac{24}{40} = 5:1$. Apparently, both setups have a lower and upper meshing frequency. For our analyses, the datasets of spur 1, spur 2, spur 4, helical 1, helical 2 and helical 5 are selected because they are healthy, small and large fault cases as depicted in Table 2.

As can be seen in Table 2, there are chipped and eccentric gears in spur 2 and broken and eccentric gears in spur 4. Eccentric gears allow the rotation of one gear to modulate the speed of the other gear which causes sidebands at the meshing frequency [20]. The resulting pattern of sidebands about the meshing frequency is generally asymmetric at multiples of the shaft speed because the motion that occurs is a combination of both amplitude and frequency modulation. A large number of high-level sidebands can indicate eccentric gears, gear tooth cracks, gear housing cracks, misaligned shafts, excessive shaft deflection etc. Based on this, it is expected that the eccentric, chipped and broken gears will all generate sidebands in the frequency spectrum.

Figures 5–10 show the vibration spectra obtained for both the spur gearbox and helical gearbox with their corresponding SR signals on the right hand side of the plot and non-SR signals on the left hand side of the plot. Each figure has an upper section corresponding to the spectrum for the lower meshing frequency range and a lower section corresponding to the spectrum for the upper meshing frequency range. The red and magenta lines represent the theoretical position of the sidebands around their corresponding fundamental frequencies. The meshing frequencies of the spur gear setup are 480 Hz and 960 Hz while that of the helical gear setup are 240 Hz and 480 Hz. A closer look at the raw figures shows a very slight deviation of the meshing frequencies from their actual values ranging from 0.21 to 0.35%. This is quite reasonable and is most likely due to the approximation to an integer of the actual shaft speed obtained during the measurement process. The figures shown here consider these deviations in the computation of the sideband positions.

In the spur gear setup of Figures 5 and 6, the very conspicuous sidebands in the non-SR signals are spaced at a shaft speed of 10 Hz, which corresponds, to the intermediate shaft where the eccentric gear is mounted. The chipped gear rotates at a shaft speed of 30 Hz while the broken gear rotates at a shaft speed of 6 Hz. The broken and chipped gear sidebands are not very discernible in Figures 5 and 6 for both data from channel 1 (input side accelerometer) and channel 2 (output side accelerometer). This could be either due to the position of both sensors or the "overshadowing" effect of the eccentric gear. In the helical gear setup of Figures 8 and 9 where there is no eccentric gear, the sidebands corresponding to the chipped and broken gears

**Table 2.** showing the different configurations and fault severities of the double stage reduction gearbox.

| Gears | | | | | Bearings | | | | | | Shafts | |
|---|---|---|---|---|---|---|---|---|---|---|---|---|
| | 32 teeth | 96 teeth | 48 teeth | 80 teeth | Input shaft: input side | Idler shaft: input side | Output shaft: input side | Input shaft: output side | Idler shaft: output side | Output shaft: output side | Input | Output |
| Spur 1 – (healthy case) | Good | Good | Good | Good | Good | Good | Good | Good | Good | Good | Good | Good |
| Spur 2 – (chipped tooth case) | Chipped | Good | Eccentric | Good | Good | Good | Good | Good | Good | Good | Good | Good |
| Spur 4 – (broken tooth case) | Good | Good | Eccentric | Broken | Ball | Good | Good | Good | Good | Good | Good | Good |

| Gears | | | | | Bearings | | | | | | Shafts | |
|---|---|---|---|---|---|---|---|---|---|---|---|---|
| | 32 teeth | 96 teeth | 48 teeth | 80 teeth | Input shaft: input side | Idler shaft: input side | Output shaft: input side | Input shaft: output side | Idler shaft: output side | Output shaft: output side | Input | Output |
| Helical 1 – (healthy case) | Good | Good | Good | Good | Good | Good | Good | Good | Good | Good | Good | Good |
| Helical 2 – (chipped tooth case) | Good | Good | Chipped | Good | Good | Good | Good | Good | Good | Good | Good | Good |
| Helical 5 – (broken tooth case) | Good | Good | Broken | Good | Good | Good | Good | Good | Inner | Good | Good | Good |

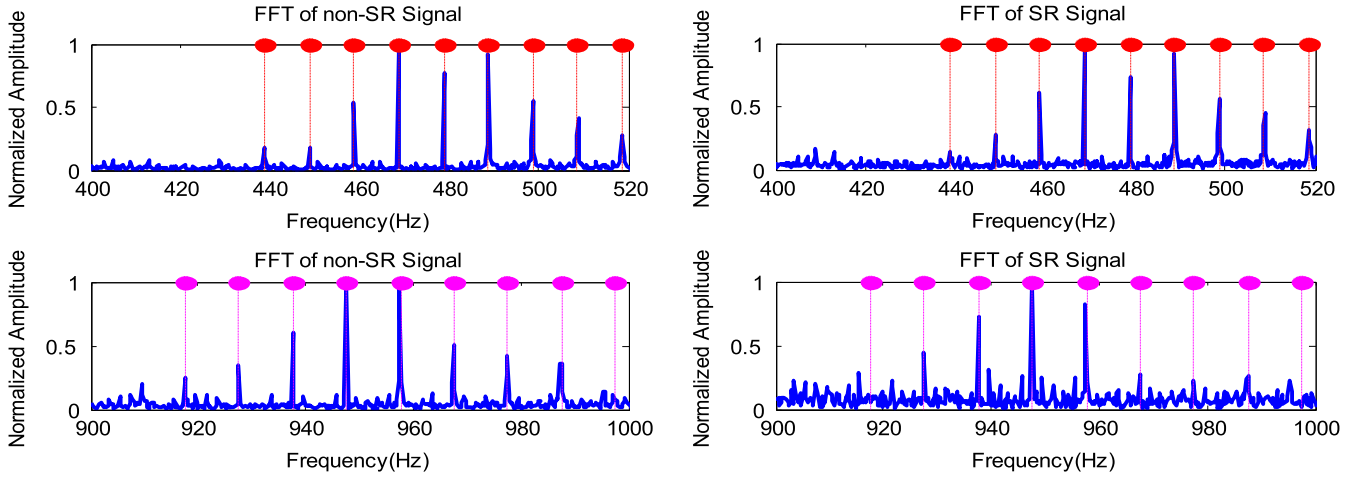


**Fig. 5.** Non-SR and SR vibration spectrum of a 1800 rpm double stage reduction spur gearbox–broken tooth case (a) lower meshing frequency range (b) upper meshing frequency range.

are distinctly visible. It should be noted that data from both channel 1 and channel 2 are quite similar but only the data from channel 2 is shown in this paper.

Comparing the non-SR signal and SR signal of Figure 5, there is no obvious difference between them. In Figure 6, the SR signal appears noisy in the lower meshing frequency range

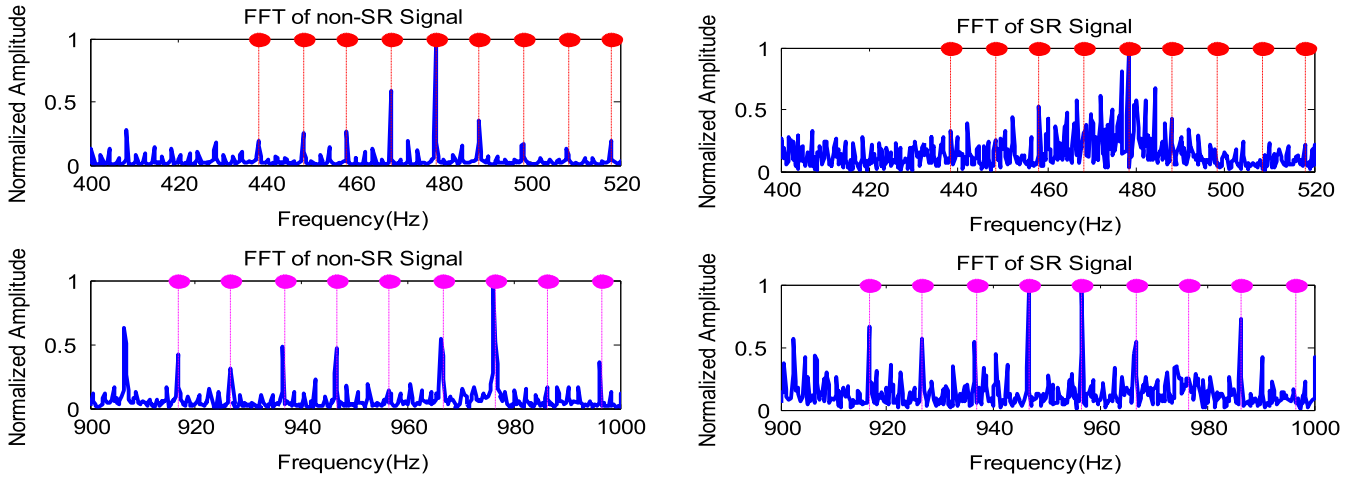


**Fig. 6.** Non-SR and SR vibration spectrum of a 1800 rpm double stage reduction spur gearbox–chipped tooth case (a) lower meshing frequency range (b) upper meshing frequency range.

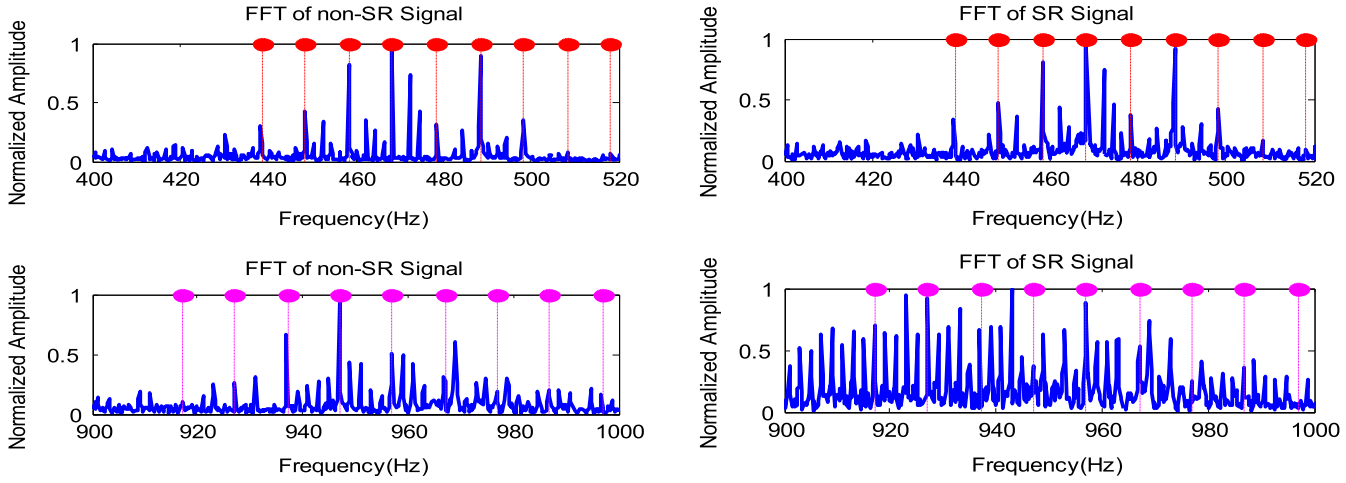


**Fig. 7.** Non-SR and SR vibration spectrum of a 1800 rpm double stage reduction spur gearbox–healthy tooth case (a) lower meshing frequency range (b) upper meshing frequency range.

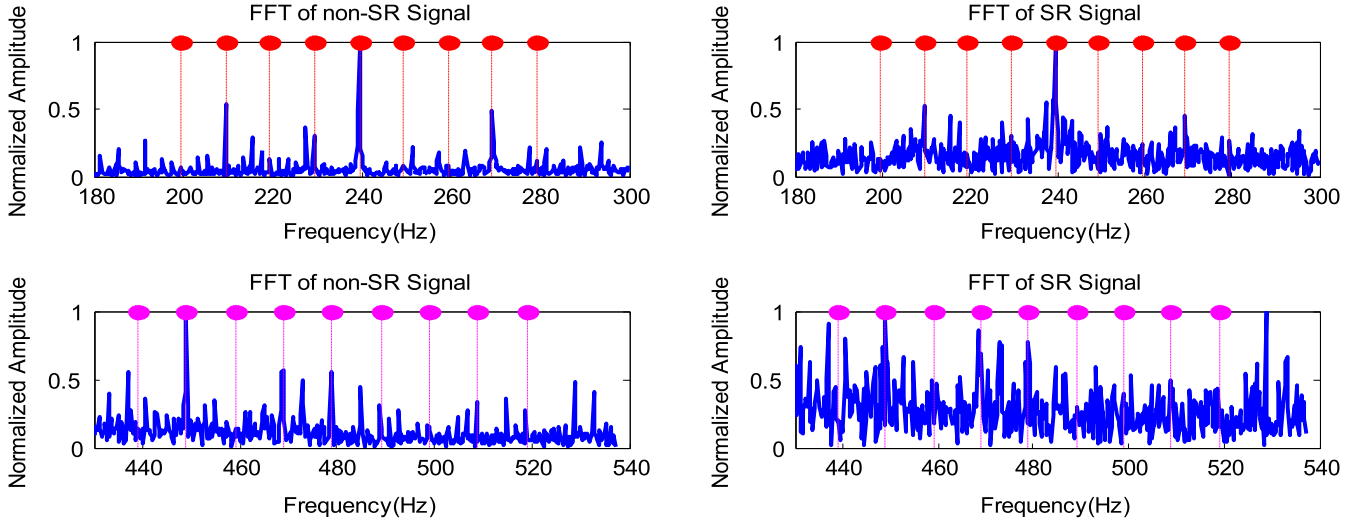


**Fig. 8.** Non-SR and SR vibration spectrum of a 1800 rpm double stage reduction helical gearbox–broken tooth case (a) lower meshing frequency range (b) upper meshing frequency range.

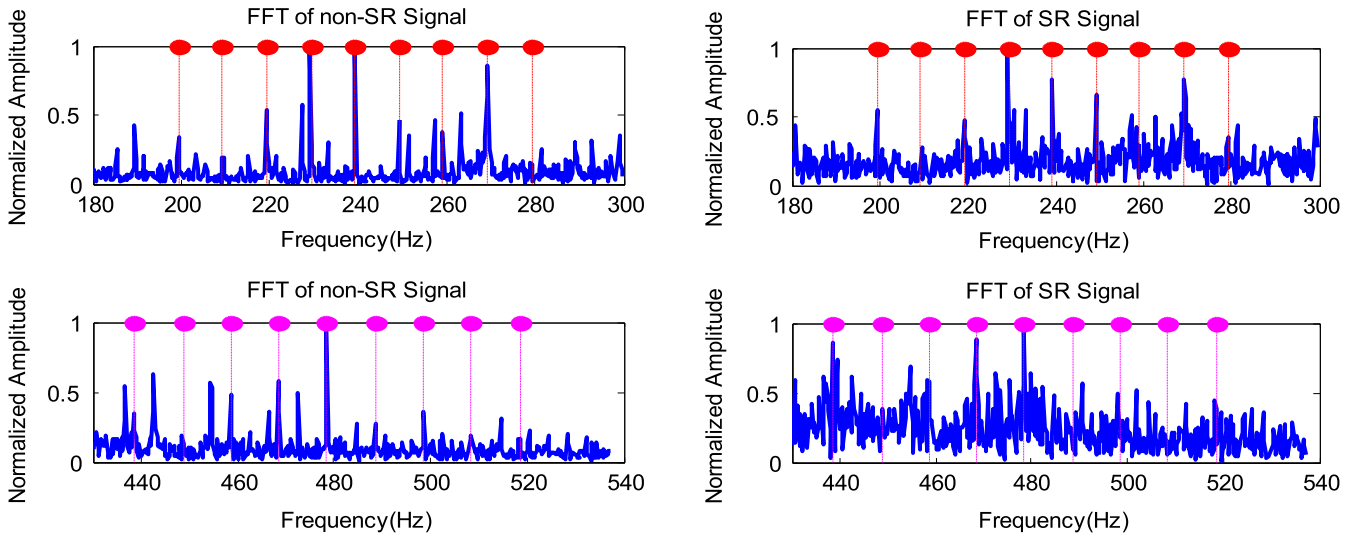


**Fig. 9.** Non-SR and SR vibration spectrum of a 1800 rpm double stage reduction helical gearbox–chipped tooth case (a) lower meshing frequency range (b) upper meshing frequency range.

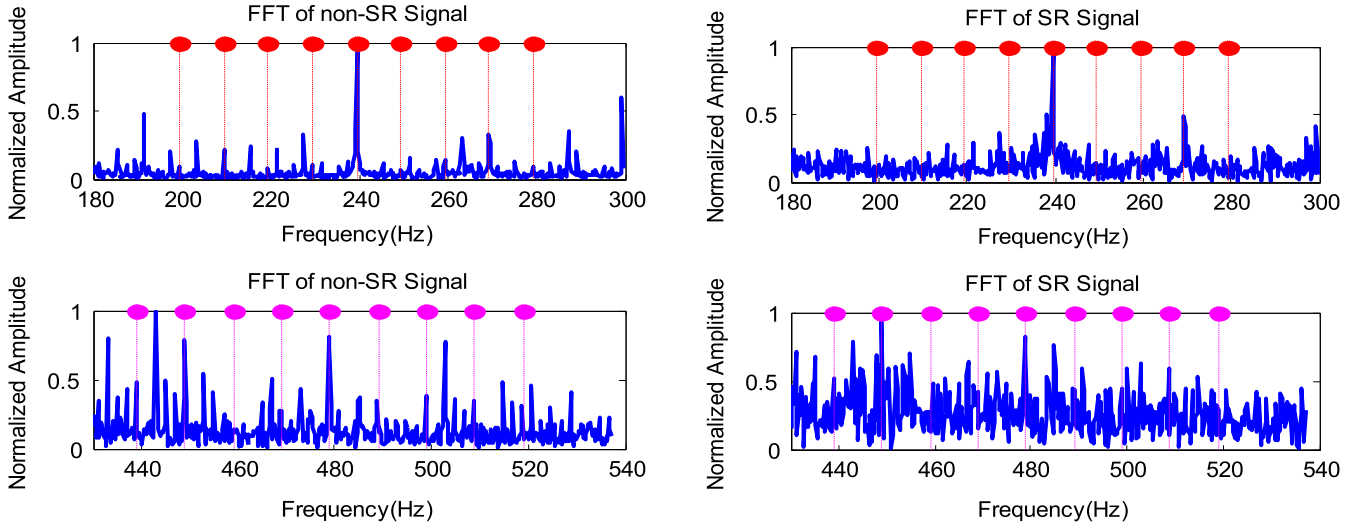


**Fig. 10.** Non-SR and SR vibration spectrum of a 1800 rpm double stage reduction helical gearbox–healthy tooth case (a) lower meshing frequency range (b) upper meshing frequency range.

while there is an amplification of eccentric gear sidebands in the higher meshing frequency range. In the healthy case of Figure 7, there is not a lot of difference between the non-SR and SR signal in the lower meshing frequency range, nevertheless, there is a huge amplification of sidebands in the higher meshing frequency range.

In the helical gear configuration, there appears to be amplification in the higher meshing frequency range of the SR signal in Figure 8 although it looks noisy. The SR signal in the lower meshing frequency is similar although a bit noisier than its corresponding non-SR signal. In Figure 9, there is amplification at 200 Hz and 250 Hz in the lower meshing frequency range of the SR signal. The other sidebands in the SR signal have either the same amplitude or lower amplitude than those in the non-SR signal. In the higher meshing frequency range of the same figure, the amplitudes of all the sidebands of the SR signal seem to be amplified even though they appear noisy. The healthy case of Figure 10 shows the SR signal having a slight amplification at 270 Hz in the lower meshing frequency range and a general amplification in the SR signal of the higher meshing frequency range.

In an overall sense, there always seems to be amplification in the SR signals with the amplifications in the higher meshing frequency range looking more noticeable and noisy. The amplification of sidebands in the healthy signals appears to be more apparent in the experimental case than the numerical simulation case in [4]. It is a well-known fact that experimental data have more noise, vibration and complexity and as a result, they could be more difficult to analyse properly. In order to solve this problem, the authors thought it necessary to reduce the complexity of the data to allow for its easier investigation. Based on this reasoning, 2 approaches are proposed to achieve this objective. The first approach

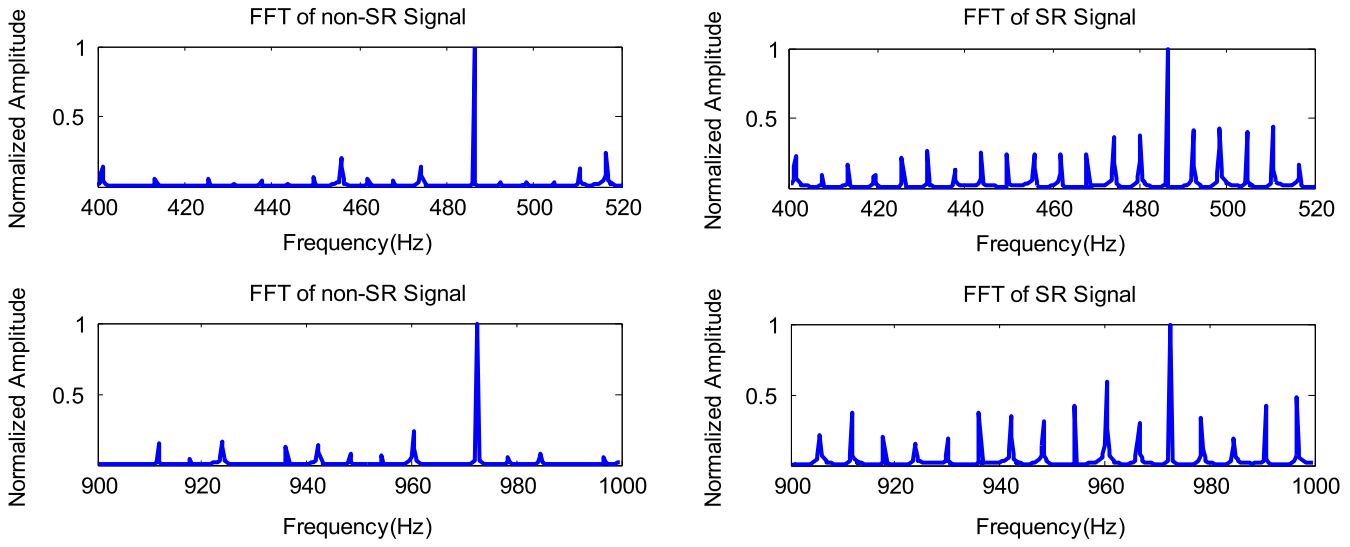


**Fig. 11.** Non-SR and SR residual signal vibration spectrum of a 1800 rpm double stage reduction spur gearbox–broken tooth case (a) lower meshing frequency range (b) upper meshing frequency range.

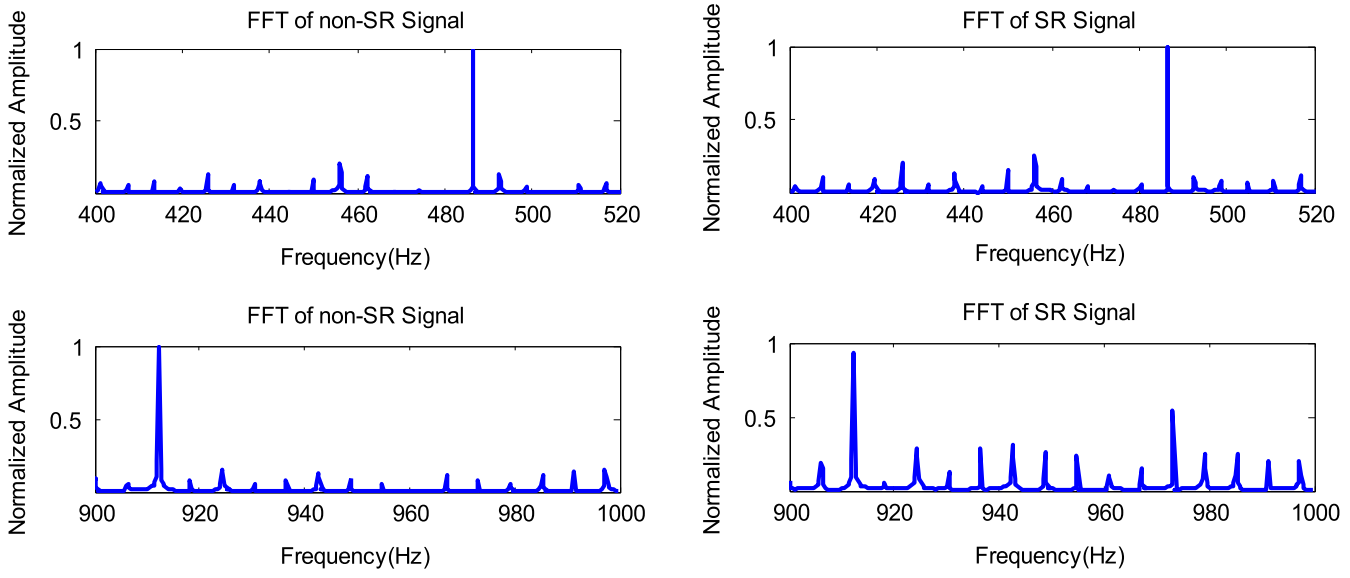


**Fig. 12.** Non-SR and SR residual signal vibration spectrum of a 1800 rpm double stage reduction spur gearbox–chipped tooth case (a) lower meshing frequency range (b) upper meshing frequency range.

involves applying SR to a residual signal rather than the raw signal while the second approach involves applying a high pass filter after selecting a proper cut-off frequency to the raw signal before applying SR. Removal of some frequencies is what both approaches have in common which makes the resulting signal less complex to examine.

### 3.1 Applying stochastic resonance to residual signals

The residual signal is determined by removing the meshing frequencies and the shaft frequencies along with their harmonics from the original time synchronous averaged (TSA) signal [14–16].

$$r = x(t) - x_r(t), \tag{5}$$

where $r$ is the residual signal, $x(t)$ is the original TSA and $x_r(t)$ is the signal containing the meshing frequencies, shaft frequencies and their harmonics. When the first order sidebands about the meshing frequency are removed from the residual signal, a difference signal is formed.

$$d = r - (f_m \pm \omega_i), \quad i = 1, \tag{6}$$

where $d$ is the difference signal, $f_m$ is the signal meshing frequency and $\omega$ is the shaft frequency. Both the residual and difference signal were proposed in order to better observe the changes that occur in a vibration signal [14].

To obtain the residual signal in this situation, 6 Hz, 10 Hz and 480 Hz, as well as their multiples are removed from the original TSA. This is sufficient to remove all the

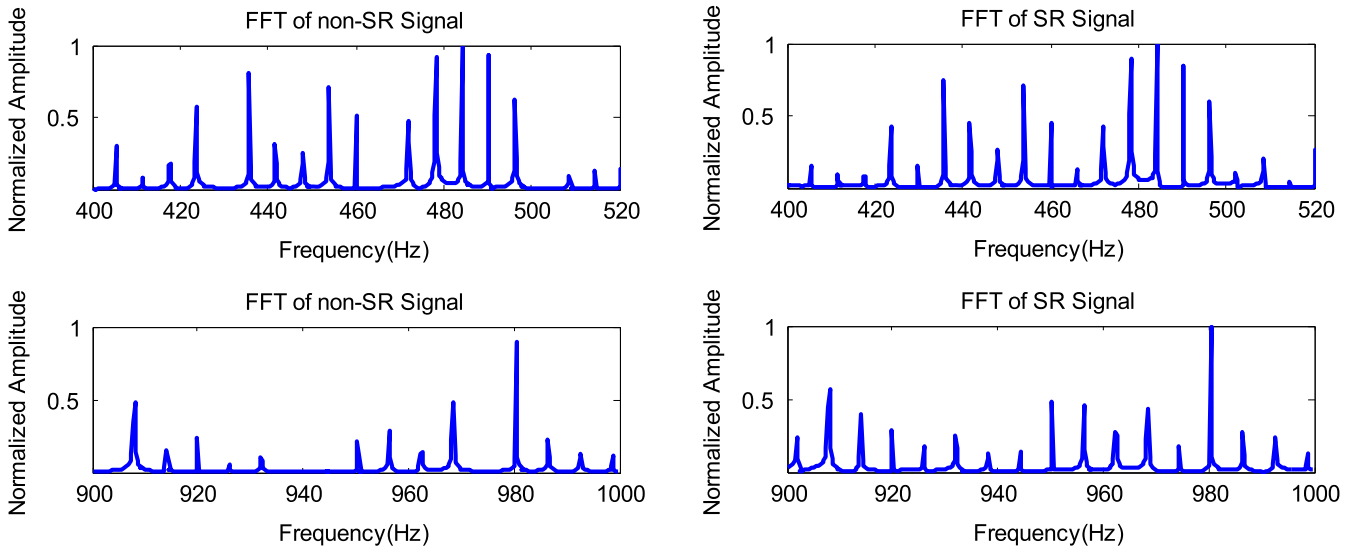


**Fig. 13.** Non-SR and SR residual signal vibration spectrum of a 1800 rpm double stage reduction spur gearbox–healthy tooth case (a) lower meshing frequency range (b) upper meshing frequency range.

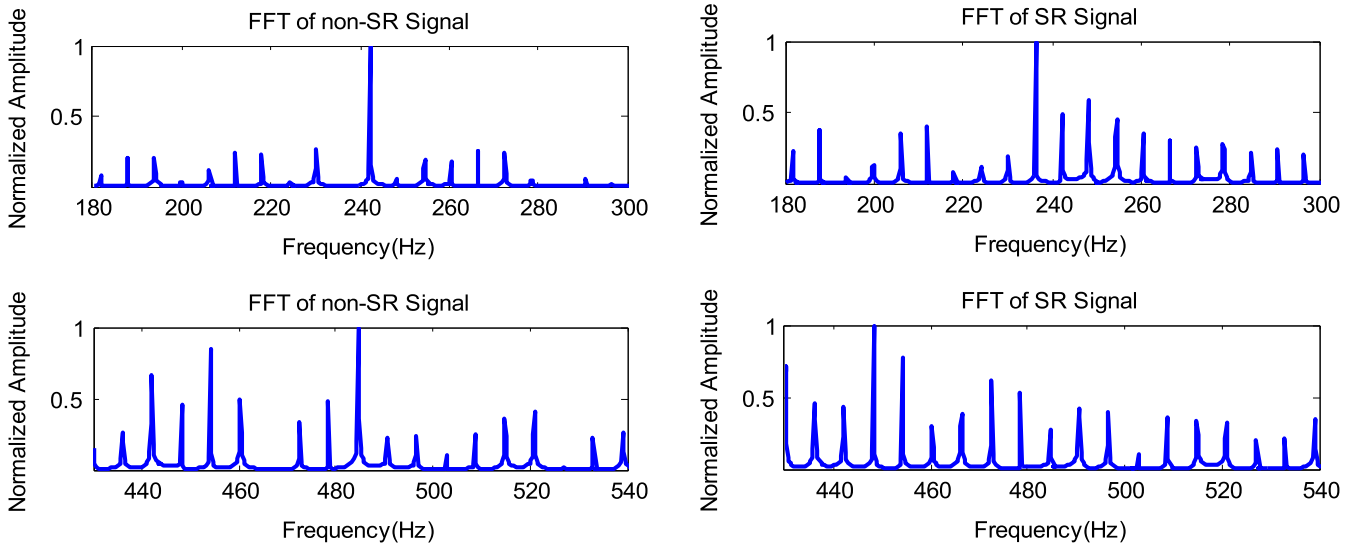


**Fig. 14.** Non-SR and SR residual signal vibration spectrum of a 1800 rpm double stage reduction helical gearbox–broken tooth case (a) lower meshing frequency range (b) upper meshing frequency range.

meshing frequencies, shaft frequencies and their harmonics since they are multiples of each other. It should be noted that the difference signal and residual signal for the experimental spur gear set up are equivalent because the first order sidebands are multiples of the shaft speeds.

In Figure 11, where there is an eccentric gear and a gear with broken tooth, the frequency spikes are very evident in both the lower and upper meshing frequency range. The frequency spikes in the lower meshing frequency range are due to the eccentric and broken tooth gears while the spikes in the upper meshing frequency range are most likely as a result of the harmonics of the spikes in the lower meshing frequency range. The frequency spikes are just as evident in the SR signal of Figure 12 especially in the higher meshing frequency range. The spikes that are present in the lower meshing frequency range are most likely due to the eccentric gear which are not as conspicuous as the spikes in the higher meshing frequency range which are most likely due to the chipped gear. In the healthy case in Figure 13, both the SR and non-SR signals are similar.

Figures 14–16 show the results when the exact same methodology is applied to the residual signal of the helical gear set up. Just like the spur gear setup, the difference signal and residual signal are equal to each other. As can be seen in Figure 14, there is a clear amplification in the lower meshing region of the SR signal due to the broken helical gear tooth particularly after the fundamental frequency. There is also amplification in the higher meshing frequency range of the SR signal at 450 Hz.

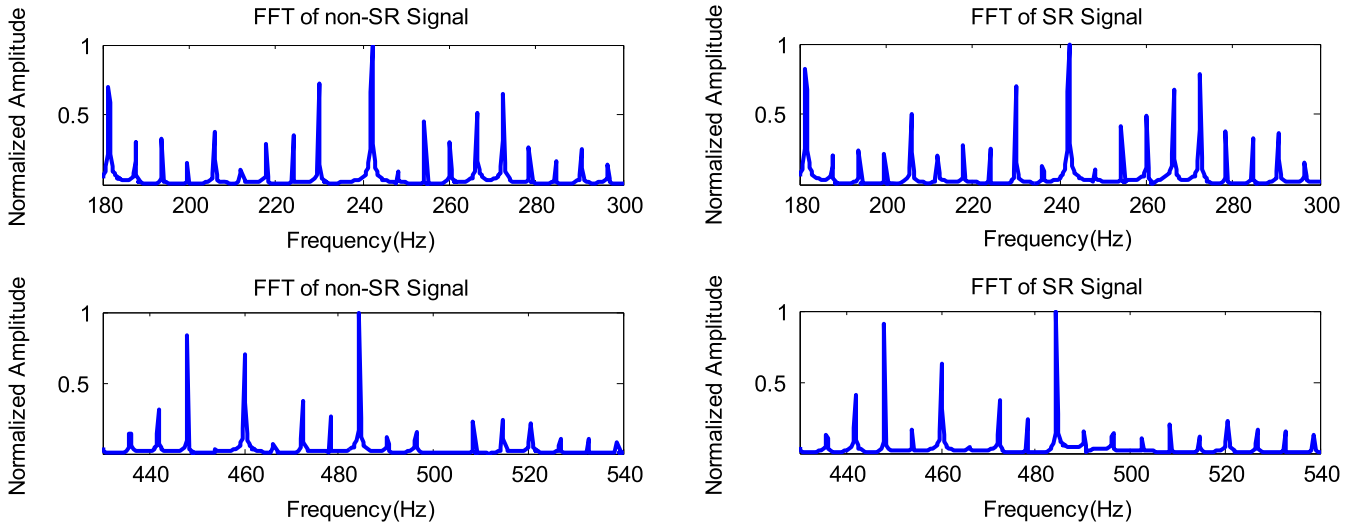


**Fig. 15.** Non-SR and SR residual signal vibration spectrum of a 1800 rpm double stage reduction helical gearbox–chipped tooth case (a) lower meshing frequency range (b) upper meshing frequency range

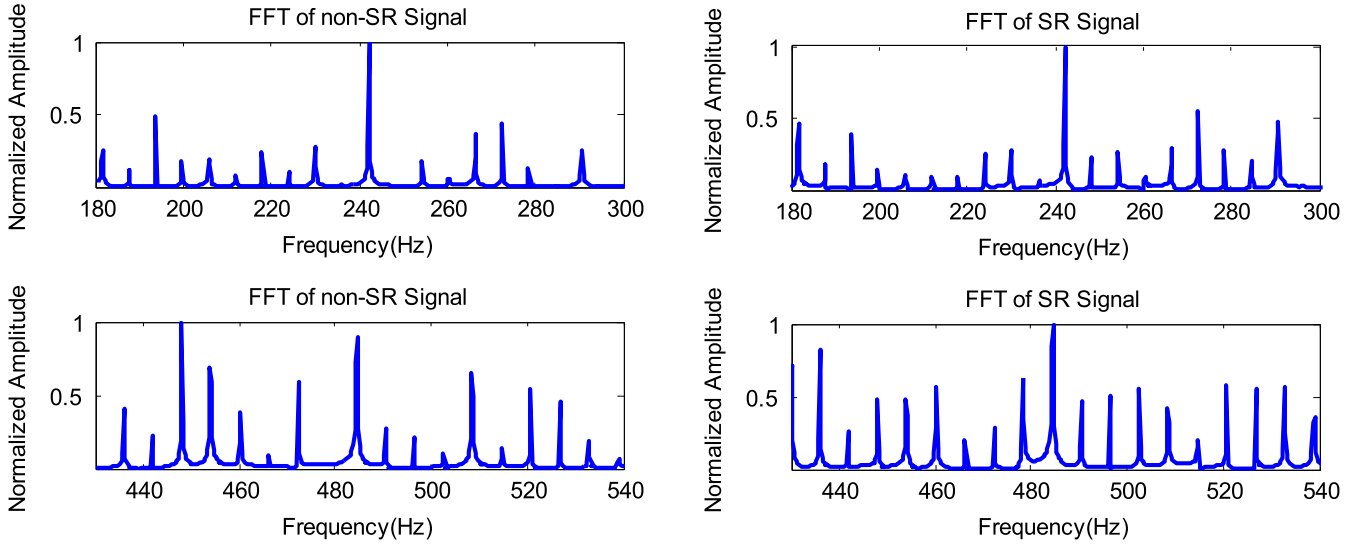


**Fig. 16.** Non-SR and SR residual signal vibration spectrum of a 1800 rpm double stage reduction helical gearbox–healthy tooth case (a) lower meshing frequency range (b) upper meshing frequency range.

In Figure 15, a quick look suggests no amplification in the SR signals but a closer look at the lower meshing frequency range shows amplification in the SR signal after the fundamental frequency. In Figure 16, the SR and non-SR signal bear close resemblance with a small amplification in the higher meshing frequency range.

It should be noted that in all the residual signal results, the frequency spacings are not regular for the non-SR signals while they are regular and spaced at 6 Hz for the SR signal.

The results of applying SR to the residual signal for experimental data are easier to interpret as compared to when SR is applied directly to the raw signal. The noisy nature of the SR signal, which is a core part of the results obtained when SR is applied directly to the raw data, disappears completely in the residual signal case. Moreover, the spikes due to faults present in the non-SR signal are more apparent and plain in the SR signals of the residual signal. This indicates that SR gives better and more comprehendible results when it is applied to a pre-treated signal.

### 3.2 Applying stochastic resonance to high-pass filtered signals

The spectra results above indicate the potential of SR as a powerful tool for vibration based condition monitoring. In the time domain however, in the absence of signal pre-treatment, the SR output of all the experimental data of the healthy gears gives a high kurtosis. This is not the case for the numerical simulations [3] described in the introduction, which give a low kurtosis when SR is applied to the healthy gear signal. As indicated earlier, the most reasonable

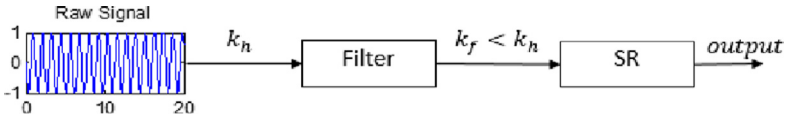


**Fig. 17.** Schematic diagram showing a possible way of choosing the high-pass filter cut-off frequency.

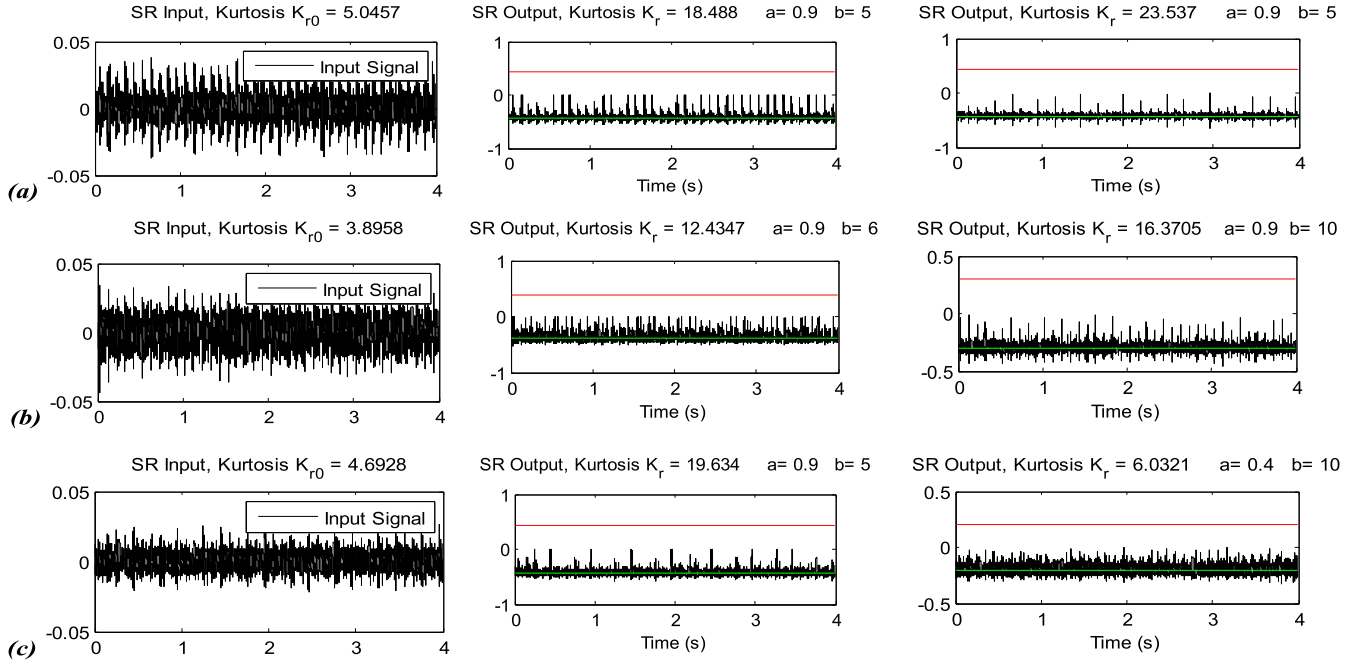


**Fig. 18.** Time histories of the non-linear dynamic system–experimental results for the spur gear setup (1st column) raw signal (2nd column) SR signal (3rd column) filtered SR signal. (1st row) broken tooth case (2nd row) chipped tooth case (3rd row) healthy case.

explanation for this phenomenon is that experimental data has more vibration, noise and complexity that makes it difficult to properly examine. Thus, it is imperative to make the signal to be analysed "less complex" before analysis.

In this section, a high-pass Butterworth filter with a proper cut-off frequency is used to achieve the said goal. Bearing in mind that SR tends to amplify the kurtosis of a signal, the cut-off frequency of the filter is selected in such a way that the kurtosis of the filtered signal is about 90% (slightly less) of the kurtosis of the original signal using the healthy case as reference. This is depicted schematically in Figure 17.

The raw signal in Figure 17 is a healthy signal, which is used as a reference. $k_h$ is the kurtosis of the healthy signal and $k_f$ is the kurtosis of the filtered signal. The value of the cut-off frequency of the filter that coincides with $k_f$ slightly lower than $k_h$ should be selected. It should be noted that the primary goal here is to contain false alarms in the time domain.

For our case, 0.216 is selected as the normalized cut-off frequency of the high-pass Butterworth filter. In Figures 18 and 19, the first column displays the raw signals, the second column displays the SR output without filtering and the third column displays the SR output after filtering. The green and red lines in the second and third columns correspond to the negative well, which is defined as $-\sqrt{a/b}$ and the positive well which is defined as $\sqrt{a/b}$ respectively of the SR output. In third column of Figures 18(a) and (b), the kurtosis of the filtered SR output is more amplified when compared with their corresponding second columns. In Figure 18c, the kurtosis of the filtered SR output in the third column is much lower than the kurtosis of the SR output in the second column. These results demonstrate that false alarms in the time domain can be contained in SR output when the raw signal is filtered before passing it through the SR dynamic system. These results are also further supported by the experimental results for the helical gear setup as seen in Figure 19. In Figure 19(a), the kurtosis of the filtered SR output of the third column is raised by a very considerable amount in comparison to the ordinary SR output of the second column. In Figure 19(b), the kurtosis for the filtered SR output in the third column is lower than its counterpart in the second column; however, the information in the third column is sufficient to identify a fault in the system. In the third column of Figure 19(c), the kurtosis of the filtered SR output is considerable lower than the kurtosis of the SR output in the second column, which demonstrates a containment of false alarms.

## 4 Conclusions

Although few researches have been done on applying SR to mechanical problems, much of the already done research focuses on faulty cases. In this paper, an all-round approach

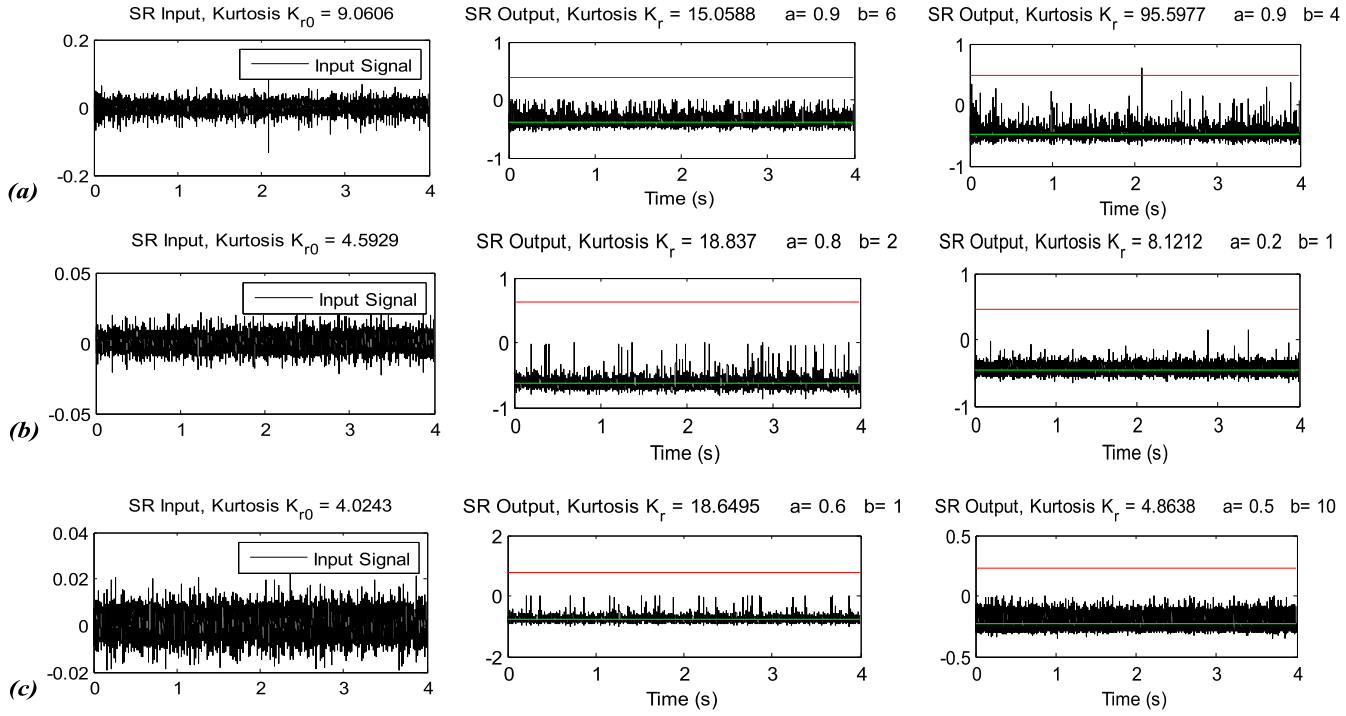


**Fig. 19.** Time histories of the non-linear dynamic system–experimental results for the helical gear setup (1st column) raw signal (2nd column) SR signal (3rd column) filtered SR signal. (1st row) broken tooth case (2nd row) chipped tooth case (3rd row) healthy case.

is taken in analysing the effect of SR on data from gearboxes including applying SR to gearbox diagnostic statistical tools. First of all, SR is applied to the raw vibration signal that is obtained from a real life gear box that has different health conditions. While SR is able to amplify the impulses in the faulty cases, it gives off false alarms in the healthy cases by a huge amplification of the vibration signal. The fact that this does not happen in the numerical simulations implies that the complexity of experimental signals might be responsible for this phenomenon. Thus, two strategies are employed in this work to tackle the problem of realistic data complexity which seems to affect the SR results. The first procedure involves computing the residual signals from the raw signals and then applying SR; the second approach involves computing the high pass filtered signal from the raw signal and then applying SR. Finally, the results obtained when SR is applied to the pre-processed signals i.e. the residual signals and high pass filtered signals, rather than the raw signals is positive as can be seen in the final sections of this paper.

## References


[1] R. Yan, R. Zhao, R.X. Gao, Noise-assisted data processing in measurement science: part one part 40 in a series of tutorials on instrumentation and measurement, IEEE Instrum. Meas. Mag. 15 (2012) 41–44

[2] S. Marchesiello, A. Fasana, L. Garibaldi, Best parameter choice of stochastic resonance to enhance fault signature in bearings, in: International Conference on Structural Engineering Dynamics, Lagos, Portugal, 2015, pp. 1–7

[3] C.U. Mba, S. Marchesiello, A. Fasana, L. Garibaldi, Vibration based condition monitoring of spur gears in mesh using stochastic resonance, in: Surveillance 8 International Conference, Roanne, France, 2015, pp. 1–15

[4] C.U. Mba, S. Marchesiello, A. Fasana, L. Garibaldi, Fault detection in gears using stochastic resonance, in: Advances in Condition Monitoring of Machinery in Non-Stationary Operations, Springer, Cham, 2018, pp. 55–70

[5] Y.G. Leng, et al., Numerical analysis and engineering application of large parameter stochastic resonance, J. Sound Vibration 292 (2006) 788–801

[6] Y. Lei, et al., Planetary gearbox fault diagnosis using an adaptive stochastic resonance method, Mech. Syst. Signal Process. 38 (2013) 113–124

[7] http://www.phmsociety.org/references/datasets, PHM Challenge Competition Data Set, 2009

[8] R. Benzi, A. Sutera, A. Vulpiani, The mechanism of stochastic resonance, J. Phys. A: Math. General 14 (1981) L453

[9] M.D. McDonnell, D. Abbott, What is stochastic resonance? Definitions, misconceptions, debates, and its relevance to biology, PLoS Comput. Biol. 5 (2009) e1000348

[10] L. Gammaitoni, P. Hänggi, P. Jung, F. Marchesoni, Stochastic resonance, Rev. Modern Phys. 70 (1998) 223

[11] X.-h. Chen, G. Cheng, X.-l. Shan, X. Hu, Q. Guo, H.-g. Liu, Research of weak fault feature information extraction of planetary gear based on ensemble empirical mode decomposition and adaptive stochastic resonance, Measurement 73 (2015) 55–67

[12] K. Worden, I. Antoniadou, S. Marchesiello, C. Mba, L. Garibaldi, An illustration of new methods in machine condition monitoring, Part I: stochastic resonance, J. Phys.: Conf. Ser. 842 (2017) 1–10

[13] X. Zhang et al., An adaptive stochastic resonance method based on grey wolf optimizer algorithm and its application to machinery fault diagnosis, ISA Trans. 71 (2017) 206–214
[14] P.D. Samuel, D.J. Pines, A review of vibration-based techniques for helicopter transmission diagnostics. J. Sound Vibration 282 (2005) 475–508
[15] M. Lebold et al., Review of vibration analysis methods for gearbox diagnostics and prognostics. in: Proceedings of the 54th Meeting of the Society for Machinery Failure Prevention Technology, 2000
[16] P. Večeř, M. Kreidl, R. Šmíd, Condition indicators for gearbox condition monitoring systems, Acta Polytech. 45 (2005) 35–43
[17] K. Christian et al., On the use of time synchronous averaging, independent component analysis and support vector machines for bearing fault diagnosis, in: First International conference on Industrial Risk Engineering, Montreal. (December 2007) 610–624
[18] E. Bechhoefer, M. Kingsley, A review of time synchronous average algorithms, in: Annual Conference of the Prognostics and Health Management Society, San Diego, California, 2009, pp. 24–33
[19] R.B. Randall, J. Antoni, Rolling element bearing diagnostics-a tutorial, Mech. Syst. Signal Process. 25 (2011) 485–520
[20] S. Goldman, Vibration spectrum analysis: a practical approach, Industrial Press Inc, 1999

**Cite this article as**: C.U. Mba, S. Marchesiello, A. Fasana, L. Garibaldi, Gearbox damage identification and quantification using stochastic resonance, Mechanics & Industry **18**, 805 (2017)